[3] N. Marcuvitz, *Waveguide Handbook* (MIT Rad. Lab. Ser., vol. 10). New York: McGraw-Hill, 1951.
[4] J. S. Joshi and J. A. F. Cornick, "Analysis of a waveguide mounting configuration for electronically tuned transferred-electron-device oscillators and its circuit application," *IEEE Trans. Microwave Theory Tech.*, vol. MTT-24, pp. 573–584, Sept. 1976.
[5] R. L. Eisenhart and P. J. Khan, "Theoretical and experimental analysis of a waveguide mounting structure," *IEEE Trans. Microwave Theory Tech.*, vol. MTT-19, pp. 706–719, Aug. 1971.
[6] J. S. Joshi, "Analysis of general waveguide post configurations," Ph.D. dissertation, Council for National Academic Awards, London, May 1976.

Double Circulation Frequency Operation of Stripline *Y*-Junction Circulators

TSUKASA NAGAO, MEMBER, IEEE

Abstract—**The double circulation frequency operation (DCFO) of stripline *Y*-junction circulators loaded with dielectric–ferrite composites is presented. The dielectric–ferrite composite is made by combining a dielectric puck with a ferrite ring. The DCFO is identified in the mode chart, and it is found that mode 1 and mode 1A, according to Davies and Cohen, play their respective roles in the circulation. Theoretical results of perfect circulation are derived, applying Bosma's Green's function to the junction mode impedances, and then, design and operation of the DCFO are studied. Finally, experimental examples are presented.**

I. Introduction

THE stripline *Y*-junction circulator has long been widely used as one of the versatile microwave devices. It can be used as an isolator or as a switch, as well as a circulator. There are really many varieties of the circulator utilized: stripline and microstrip versions, *Y* and *X* junctions, wide-band and narrow-band uses, and so on. These varieties of the circulator are evidence that it has served various needs arising in microwave circuit design. Needless to say, it is practically important that these circulators are dealt with theoretically. As is known generally, some consistent theories are available about the elementary circulator. The design and the operating procedure of the circulator were developed by Bosma [1], [2], Davies and Cohen [3], and Fay and Comstock [4]. Many researchers have since demonstrated that they are conspicuously useful in making circulators, usually for narrow bandwidth use. If broad-banding circuits are utilized, then wide-band circulators are actually realized. Recently, Wu and Rosenbaum [5] have demonstrated that they are also effective in achieving an octave bandwidth operation of the circulator, without any broad-banding circuits.

However, it is worthwhile to note that all of these circulators are designed to operate at a single circulation frequency regardless of wide-band use or narrow-band use. Therefore, in the *Y*-junction circulators the dominant normal mode, especially mode 1 among the modes of perfect circulation, plays an essential role. As already noted by many people, a higher order mode operation is also available in a *Y* circulator or in an *X* circulator if it is adequately adjusted to its circulator conditions [3], [4], [6].

Some further efforts to enhance the versatility of the circulator have been made, which are related to the simultaneous operation of both the dominant mode and any other modes. It has not received much attention, though it is conceivably possible. There are a few examples, [7] and [8], referred to as simultaneous operation, in which one circulation takes place below the ferromagnetic resonance, and the other circulation takes place above the resonance in the sense opposite to that below the resonance. The operation of this type, however, is hard to deal with from the consistent theory of the elementary circulator because it does not hold beyond ferromagnetic resonance.

In this paper, apart from the simultaneous operation of both below-resonance and above-resonance circulations, the double circulation frequency operation (DCFO) is treated. DCFO is obviously another simultaneous operation which takes place exclusively above or below resonance, and which consists of both the dominant mode circulation and the other mode circulation. Only the DCFO above resonance is discussed.

The stripline *Y*-junction circulator used, as is shown in Fig. 1, is a stripline *Y* junction loaded with ring ferrites (dielectric–ferrite composites) in place of disk ferrites, and it is detached from any external tuning elements for the purpose of broad banding the circulator. The external magnetic field is applied parallel to the axis of the ring ferrites and the ferrite is biased beyond saturation.

To identify the DCFO, points of maximum isolation (isolation peak) are plotted superposed in the mode chart,

Manuscript received April 22, 1976; revised August 2, 1976.
The author is with the Department of Electrical Engineering, National Defense Academy, Yokosuka, Kanagawa 239, Japan.

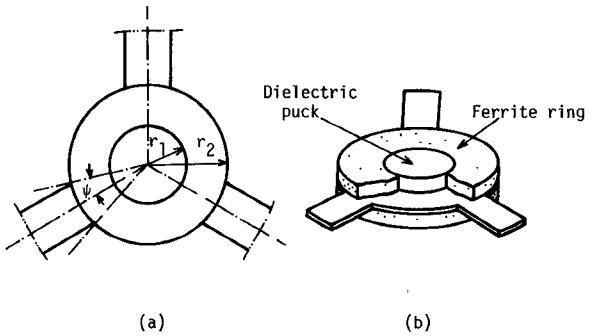

Fig. 1. (a) The configuration of the stripline Y junction. (b) Sketch of the dielectric–ferrite composite.

which results in confirmation of the validity of the constituent normal modes' description of the double circulator action.

Theoretical analysis of the DCFO is made using Bosma's Green's function, and the design procedure is discussed. It is important to note that a frequency separation between the double circulation frequencies can be controlled by taking the ratio of inner to outer radius r_1/r_2 of the ring ferrite and its saturation magnetization.

II. Identification of DCFO

The DCFO is characterized by double peaks of isolation, with minimum insertion loss. To identify the DCFO in an earlier paper [9], the double peaks were computed to be plotted directly on the chart of propagation constant-radius product k_2r_2 versus ferrite anisotropic splitting factor κ/μ, but it was inadequate for correctly making a comparison between theoretical and experimental results because of the inevitable estimation of the internal magnetic field intensity inside the ferrite ring, which caused misunderstandings. In this paper, they are plotted on the corresponding mode chart instead, as is shown in Fig. 2. The mode chart is made by measuring resonances in the ring ferrite resonator. It seems to be similar to that of the disk ferrite resonator shown by Fay and Comstock [4], except that the mode chart of the ring ferrite resonator depends on the ratio of r_1/r_2.

Curve I for the lower frequency peak goes in the vicinity of the resonance curve $n = +1$ and finally to the single circulation frequency operation (SCFO) close to the degenerate point of the modes $n = +1$ and -1 as the external magnetic field increases. Then, curve II for the higher frequency peak goes almost coincidentally with the resonance curve $n = +2$, but vanishes just before it crosses over the resonance curve $n = -1$. Curve III goes along the resonance curve $n = +3$. The same features are observed among other cases of different ratios of r_1/r_2 and different saturation magnetizations.

These comparisons in the mode chart lead to the conclusion that, according to the notation given by Davies and Cohen [3], curve I stands for mode 1, curve II for mode 1A and curve III for mode 3, among the modes of perfect circulation. It is recognized from other experiments that both resonance curves and circulation curves (curves of isolation peaks) shift toward the higher frequency, as the ratio r_1/r_2 increases and also as the saturation magnetization of the ferrite decreases.

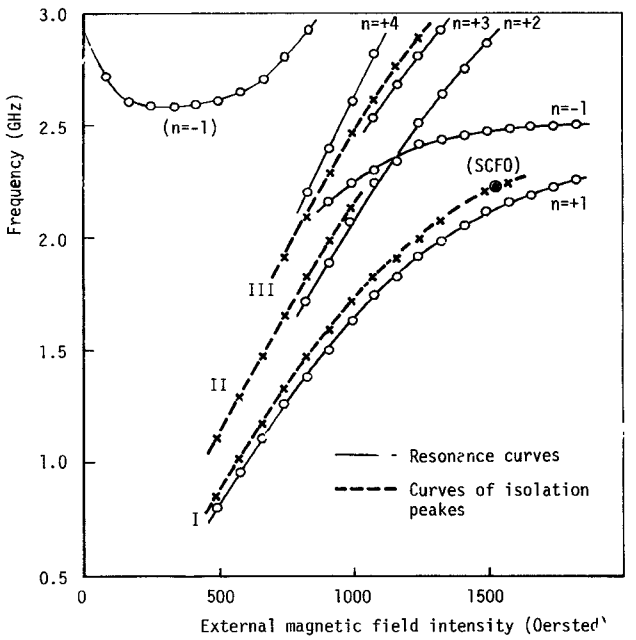

Fig. 2. Relationships between resonance curves and curves of isolation peaks superimposed on the mode chart, with the specifications that the saturation magnetization of the ring ferrite $4\pi M_s = 750$ G, the half-width $\Delta H = 80$ Oe, the specific permittivity $\varepsilon_2 = 14.5$, $r_1/r_2 = 0.45$, $r_2 = 10$ mm and the junction coupling angle $2\psi = 0.8$. A bracketed number shows a resonance curve below resonance.

III. Theoretical Analysis

A. Electromagnetic (EM) Fields and Bosma's Green's Function

The EM fields are easily derived by solving a simple eigenvalue problem describing a very thin dielectric–ferrite composite (see Appendix). In this research, the dielectric of the composite is replaced with air. Using the EM field expressions in the composite, one can construct the Green's function $G(r,\theta;r_2,\theta')$ for the wave equation satisfied by the electric field inside the ring ferrite

$$G(r,\theta;r_2,\theta') = -j\frac{Z_e}{2\pi}\sum_{\nu=-\infty}^{\infty}\frac{F_\nu(x)e^{-j\nu(\theta-\theta')}}{F_\nu'(x_3) - \dfrac{\kappa}{\mu}\dfrac{\nu}{x_3}F_\nu(x_3)} \quad (1)$$

where

$F_\nu(x)$ solution to the eigenvalue equation consisting of Bessel functions of the first kind $J_\nu(x)$ and the second kind $Y_\nu(x)$ with order ν; and especially, $F_\nu \neq F_{-\nu}$;

$F_\nu'(x)$ derivative of $F_\nu(x)$ with respect to its argument x;

x $= k_2r$ = radial wave propagation constant-radius product;

x_3 $= k_2r_2$;

k_2 $= \omega\sqrt{\varepsilon_0\mu_0\varepsilon_2\mu_e}$ = radial wave propagation constant;

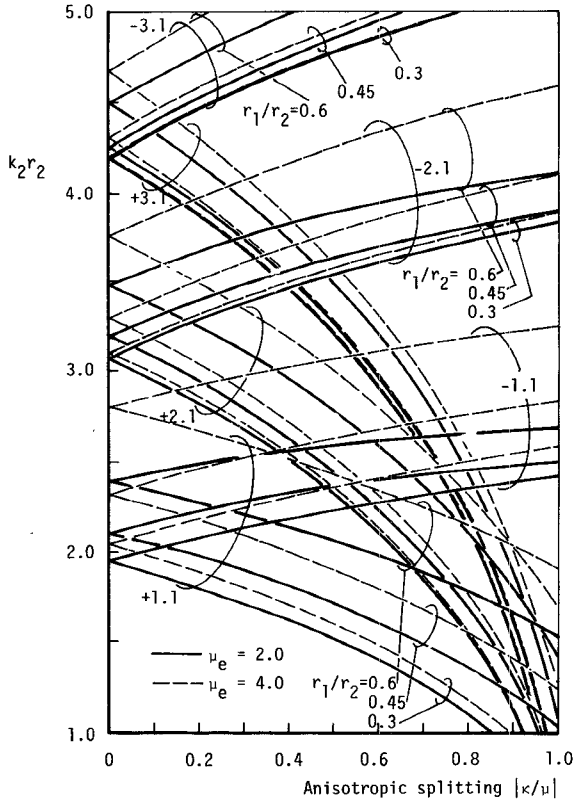

Fig. 3. The dependence on κ/μ of the k_2r_2 values of several resonant modes. The plus sign denotes a clockwise rotating mode and the minus sign a counterclockwise rotating mode. The first index refers to the order and the second to the pair number of a mode.

μ_e = $(\mu^2 - \kappa^2)/\mu$ = specific effective permeability of the ferrite;
μ,κ elements of Polder tensor [10] of the ferrite;
ε_2 specific permittivity of the ferrite;
Z_e = $\sqrt{\mu_0\mu_e/\varepsilon_0\varepsilon_2}$ = intrinsic wave impedance of the ferrite;
r_1,r_2 inner and outer radii of the ferrite ring, respectively.

The magnetic field intensity is derived from the electric field using Maxwell's equations (see Appendix).

B. Resonances

Only the resonances of the composite with a magnetically short-circuited edge have importance. They occur if the denominator of one of the terms of the series (1) becomes zero,

$$F_\nu'(x_3) - \frac{\kappa}{\mu}\frac{\nu}{x_3}F_\nu(x_3) = 0 \tag{2}$$

where ν may be any positive or negative integer. In Fig. 3, examples of the x_3 versus κ/μ relationship are shown for several modes. The dependence of the x_3 values on κ/μ is found to be similar to that for the disk configuration. In Fig. 4, another dependence on r_1/r_2 of the x_3 values is sketched, especially for the degenerate points with $\kappa/\mu = 0$.

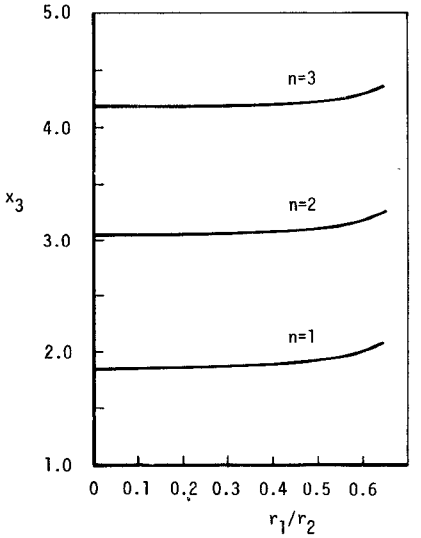

Fig. 4. The dependence on r_1/r_2 of the x_3 values of the degenerate points of several resonant modes.

One can understand that resonance curves shift upwards if r_1/r_2 increases, and also that the mode chart agrees with the resonance curve regarding the r_1/r_2 dependence.

C. Junction Mode Impedances and Circulation Conditions

The Y-junction circulation can be theoretically treated by applying Bosma's Green's function to junction mode impedances. Boundary conditions of the Y junction at the connections are simply assumed, with an approximate magnetic field applied to each port, that the tangential component is expressed by

$$H_\theta(r_2,\theta') = \begin{cases} A, & -\psi < \theta' < \psi, & \text{at port 1} \\ B, & \frac{2}{3}\pi - \psi < \theta' < \frac{2}{3}\pi + \psi, & \text{at port 2} \\ C, & -\frac{2}{3}\pi - \psi < \theta' < -\frac{2}{3}\pi + \psi, & \text{at port 3} \\ 0, & \text{elsewhere} \end{cases} \tag{3}$$

where A, B, and C are complex constants. With these approximate boundary conditions, the total electric field in the z coordinate is solved by evaluating the integral

$$E_z(r,\theta) = \int_{-\pi}^{\pi} G(r,\theta;r_2,\theta')H_\theta(r_2,\theta')\,d\theta' \tag{4}$$

where θ' is the angular coordinate located at each port with the angle 2ψ subtending the stripline width.

To obtain the junction mode impedances, corresponding boundary conditions must be applied according to its eigenvector U_j (j = 0, 1, 2). They are

$$U_0 = \begin{pmatrix}1\\1\\1\end{pmatrix} \qquad U_1 = \begin{pmatrix}1\\\omega\\\omega^2\end{pmatrix} \qquad U_2 = \begin{pmatrix}1\\\omega^2\\\omega\end{pmatrix}$$

where 1, ω, and ω^2 are the cube roots of unity. Taking E_z and H_θ to be proportional to the eigenvector elements at each port, and applying the boundary conditions (3) which are replaced with corresponding elements of each eigenvector U_j, one can obtain the respective junction mode impedance Z_j or $(E_z/H_\theta)_j$. Considering each eigensolution in turn, one can derive the following results: For $j = 0$, $A: B: C = 1: 1: 1$, therefore,

$$(E_z/H_\theta)_0 = Z^{(0)} = j\frac{\sqrt{3}\,\psi}{\pi} Z_e h_0; \tag{5}$$

for $j = 1$, $A: B: C = 1: \omega: \omega^2$, therefore,

$$(E_z/H_\theta)_1 = Z^{(+1)} = j\frac{\sqrt{3}\,\psi}{\pi} Z_e h_1; \tag{6}$$

for $j = 2$, $A: B: C = 1: \omega^2: \omega$, therefore,

$$(E_z/H_\theta)_2 = Z^{(-1)} = j\frac{\sqrt{3}\,\psi}{\pi} Z_e h_2; \tag{7}$$

where

$$\begin{cases} h_0 = \sum_{m=0}^{\infty} S(3m\psi) \dfrac{2f_{3ma}}{f_{3ma}^2 - (g_{3m} - f_{3ms})^2} \\ h_1 = \sum_{m=-\infty}^{\infty} S\{(3m+1)\psi\} \dfrac{1}{f_{3m+1} - g_{3m+1}} \\ h_2 = \sum_{m=-\infty}^{\infty} S\{(3m-1)\psi\} \dfrac{1}{f_{3m-1} - g_{3m-1}} \end{cases} \tag{8}$$

and, for all $n = 3m - 1, 3m, 3m + 1$,

$$\begin{cases} f_n = \{F_\nu'(x_3)/F_\nu(x_3)\}_{\nu=n} \\ g_n = \dfrac{\kappa}{\mu}\dfrac{n}{x_3} \\ f_{na} = (f_n + f_{-n})/2 \quad f_{ns} = (f_n - f_{-n})/2. \end{cases} \tag{9}$$

Equating each junction mode impedance with its corresponding impedance derived from the eigenvalues of the scattering matrix [3], [6], one can obtain the desired circulation condition equations given by

$$(h_0 + h_1 + h_2)(h_0h_1 + h_1h_2 + h_2h_0) - 9h_0h_1h_2 = 0 \tag{10}$$

$$\frac{\psi}{\pi}(Z_e/Z_d) = \frac{h_1 - h_2}{2h_1h_2 - h_0(h_1 + h_2)} \tag{11}$$

where ψ/π is the coupling angle ratio, Z_d is the wave impedance of the coupled stripline, and Z_e/Z_d is the junction intrinsic wave impedance ratio. The left term of (11) is the product of coupling angle and junction intrinsic wave impedance ratios. Equations (10) and (11) give the two conditions required for perfect circulation. They are essentially the same as derived by Bosma [1] and Davies and Cohen [3] if the geometry of the ferrite ring approaches a disk shape as r_1/r_2 approaches zero. The quantities h_0, h_1, and h_2 given in (8) are infinite series with each term corresponding to a particular resonant mode such as mentioned before. These infinite terms are necessary for theoretical treatment of the circulator, but not all terms are important in practical application.

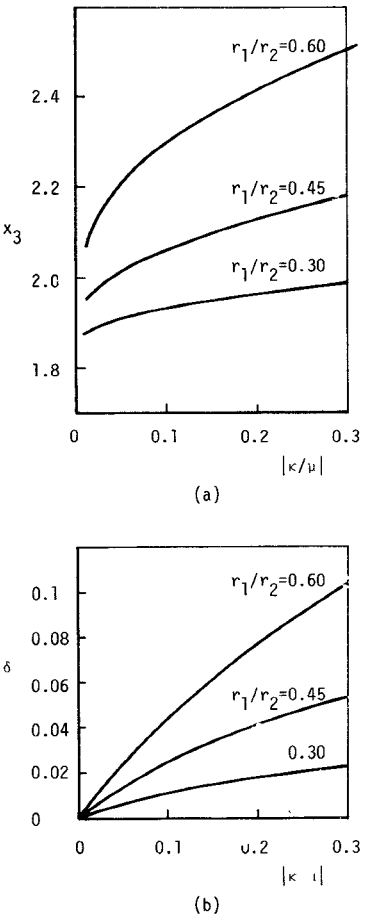

Fig. 5. (a) The relationship of x_3 versus κ/μ of mode 1 which is approximated by the $n = 1$ terms and (b) the dependence of increment ratio δ on κ/μ, with the specifications that the saturation magnetization $4\pi M_s = 950$ G and the frequency 1 GHz.

As for SCFO, the circulator is usually set close to the degenerate point of the resonant modes $n = +1$ and -1. Then if one considers only the $n = 1$ terms, the results of the first condition are given in Fig. 5(a). The second condition is reduced to

$$Z_e/Z_d = \frac{\pi}{\psi}\frac{\kappa/\mu}{x_3(1+\delta)}\frac{1}{3} \tag{12}$$

where

$$\delta = \frac{x_3 f_{1s}}{(\kappa/\mu) - x_3 f_{1s}}. \tag{13}$$

The δ values are computed in Fig. 5(b), giving an increment ratio of the perfect circulation root x_3 ($= k_2 r_2$), which is unaffected by fringing fields at the periphery of the ferrite. This only suggests that a circulator radius must be a little larger than the predicted design.

In DCFO, the one circulation of the $n = 1$ terms may be taken close to the value of the degenerate point of the modes $n = +1$ and -1, but the other can never be chosen close to any degenerate point, because both circulations must be on one locus of a particular internal magnetic field intensity along which the anisotropic splitting factor κ/μ and

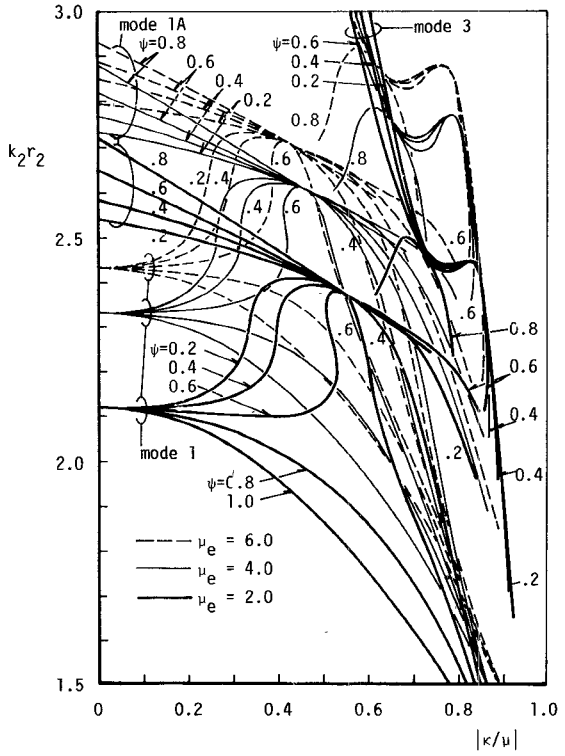

Fig. 6. Roots of the first circulation condition.

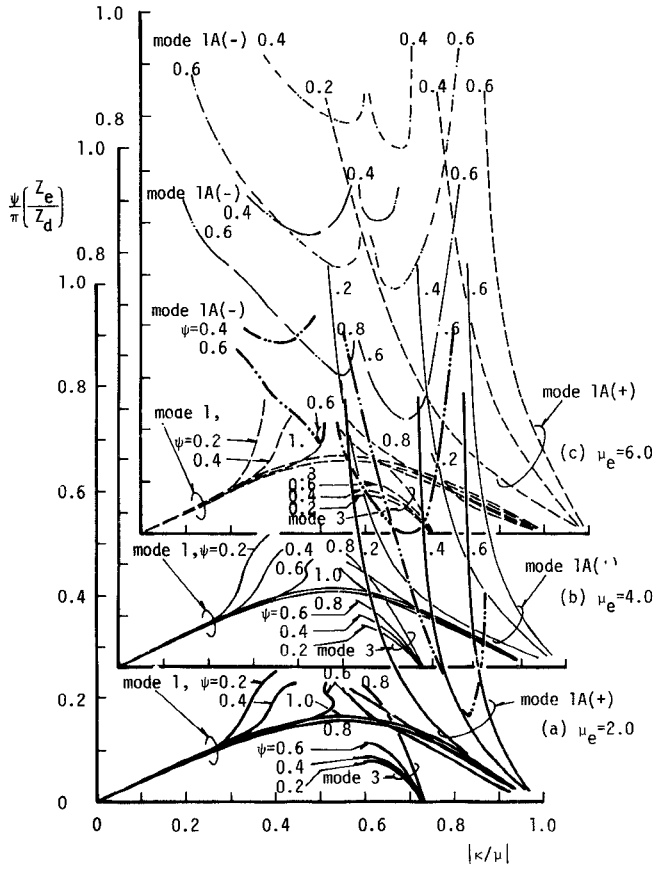

Fig. 7. The coupling angle and junction intrinsic wave impedance ratios' product $(\psi/\pi)(Z_e/Z_d)$ as a function of κ/μ calculated from the second circulation condition. The plus and minus signs of mode 1A show the positive and negative directions of circulation, respectively.

the circulation frequency vary. One cannot deduce any simple expression similar to (12) for the DCFO.

Computations of (10) and (11) are made, retaining terms up to $n = 6$. Then, the specific effective permeability μ_e is taken as an independent parameter besides the half-coupling angle ψ of the stripline and the inner-to-outer radius ratio r_1/r_2. Fig. 6 shows the solutions to the first circulation condition computed from (10). There are several sets of modes, that is, modes 1, 1A, and 3. Fig. 7 shows the solutions to the second circulation condition (11) giving the values of $(\psi/\pi)(Z_e/Z_d)$ against κ/μ. It is interesting to find out that in addition to the analogy of the first circulation condition between the ring ferrite and the disk, most of the $(\psi/\pi)(Z_e/Z_d)$ versus κ/μ relationships are smaller than the Z_e/Z_d versus κ/μ relationships of the disk configuration given by Davies and Cohen [3], Whiting [11], and Wu and Rosenbaum [5].

Mode 1 has a set of roots between the resonance curves $n = +1$ and $n = -1$, and, from the curves of its $(\psi/\pi)(Z_e/Z_d)$ versus κ/μ relationships which are shown in Fig. 7, it provides useful design data with only a positive direction of circulation. As for mode 1A, Davies and Cohen pointed out that for the disk configuration the value of Z_e/Z_d is too high for practical use except $\kappa/\mu = 0.75$. However, it is found that for the ring ferrite it has useful values of $(\psi/\pi)(Z_e/Z_d)$ within the range of the same values of mode 1 with a positive direction.

Generally speaking for DCFO, one may therefore think that there is a choice between the two combinations of mode 1 with mode 1A with a positive direction and with a negative direction. Only the combination with the same positive direction is treated in this paper. The other combination with different directions of circulation, of course, seems to be practically possible and provides the alternative version of DCFO.

D. DCFO

To operate simultaneously at two circulation frequencies, the circulator is required to satisfy the two circulation conditions at each operating point. This was demonstrated schematically in an earlier paper [9], but because the solution was only approximated by retaining the $n = 0$ and 1 terms, it was inadequate to correctly demonstrate the mechanism of DCFO. Using the results of computations of (10) and (11), we can now explain it.

Each operating point of the DCFO is found to take place under one definite internal magnetic field. In other words, they can be distinguished from each other in the k_2r_2 versus κ/μ chart of the first circulation condition on which both the constant internal magnetic field locus and, if necessary, the constant frequency locus are superimposed. These loci are derived using Polder's equations of μ and κ with a given saturation magnetization [10], and computing the k_2r_2 versus κ/μ relationship.

Fig. 8(a) shows schematically locations of the operating points in the k_2r_2 versus κ/μ chart. P_1, P_2, and P_3, respectively, show the operating points of mode 1, mode 1A, and

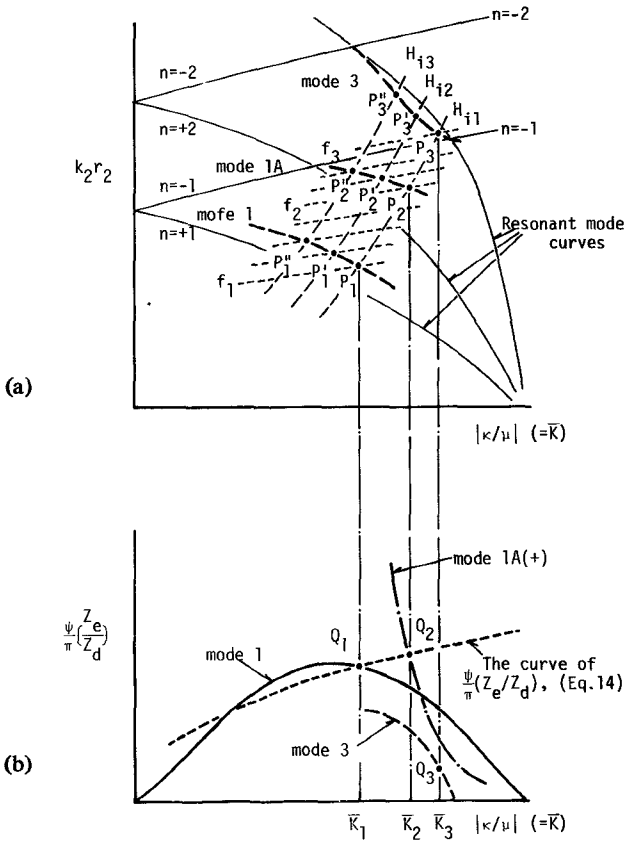

Fig. 8. Schematic performance of circulation adjustments using the two circulation conditions. (a) Results of the first circulation condition. (b) Results of the second circulation condition.

mode 3 along the internal magnetic field locus H_{i1}. If the magnetic field increases from H_{i1} to H_{i2}, each operating point moves along its mode curve, say, from P_1 to P_1', from P_2 to P_2', and so on, which depends on ψ, the half-coupling angle of the stripline. At this moment, one can tell the circulation frequencies f_1, f_2, and f_3 with respect to those points P_1, P_2, and P_3.

These operating points P_1, P_2, and P_3 are now projected at the points Q_1, Q_2, and Q_3, respectively, in the corresponding chart of $(\psi/\pi)(Z_e/Z_d)$ versus κ/μ as is shown in Fig. 8(b). It shows graphically the results of the second circulation condition. In order to satisfy the second circulation condition, the left-hand term of (11) must be equal to the right-hand term. It means that all the points Q_1, Q_2, and Q_3 on the curves of the right-hand term of (11) must be adjusted to be aligned along the curve of the coupling angle and junction intrinsic wave impedance ratios' product $(\psi/\pi)(Z_e/Z_d)$, for which one can obtain an approximate expression by taking Richardson's formula [12] for the wave impedance of the stripline. That is,

$$\frac{\psi}{\pi}(Z_e/Z_d) \simeq \sqrt{\varepsilon_d\mu_e/\varepsilon_2}\,\frac{1}{\frac{\pi r_2}{W}\log_e\left(\frac{W+D}{W+t}\right)^2} \tag{14}$$

where $W \simeq 2\psi r_2$, ε_2, and μ_e are specific permittivity and effective permeability of the ring ferrite, ε_d is the specific permittivity of a dielectric pervading a stripline, whose geometry is specified by D, the distance between the two ground planes, and W is the width and t the thickness of the center conductor.

The aforementioned circulation adjustments are completed if the operating points represented by Q_1, Q_2, and Q_3 become intersections of the curves of (14) and the $(\psi/\pi)(Z_e/Z_d)$ versus κ/μ relationships. It is, however, difficult to get the three points to simultaneously satisfy the two circulation conditions, because there is no intersection between the curve of (14) and the curve of $(\psi/\pi)(Z_e/Z_d)$ versus κ/μ of mode 3. Therefore, the operation of mode 3 fails to satisfy the second circulation condition and the DCFO appears. It seems convenient in practical use.

The circulation adjustments of the DCFO are actually achieved by changing several factors: coupling angle 2ψ of a stripline, ferrite material, dielectric pervading the stripline and that of the center puck, the radius of the ferrite, and the applied magnetic field intensity.

As for mode 3, it is recognized from Fig. 7 that the curve of $(\psi/\pi)(Z_e/Z_d)$ versus κ/μ goes straight up if the half-coupling angle ψ of the stripline is 0.8. Mode 3 has potential to satisfy the second circulation condition. Other higher order modes, of course, exist in the higher frequency region, and some of them are capable of satisfying the second circulation condition though they are not shown in Figs. 6 and 7 at all. It suggests that there exists a multiple circulation operation.

E. Input Impedance

The input impedance has importance in circulator adjustments. As it is closely related to the impedance matching of the externally coupled transmission line, it eventually affects the circulator characteristics of DCFO.

The input impedance is defined on the transverse section of the coupled stripline very close to the junction at the input port, and it can be calculated as follows. As the junction mode impedances $Z^{(0)}$, $Z^{(+1)}$, and $Z^{(-1)}$ are known, one can obtain the corresponding impedance matrix for the Y junction, and then deduce the input impedance with the other two ports terminated with the wave impedance of coupled striplines.

Rewriting the junction mode impedances as follows,

$$\begin{cases} Z^{(0)} = j\dfrac{\sqrt{3}\,\psi}{\pi} Z_e h_0 \\ Z^{(+1)} = j\dfrac{\sqrt{3}\,\psi}{\pi} Z_e h_1 \\ Z^{(-1)} = j\dfrac{\sqrt{3}\,\psi}{\pi} Z_e h_2 \end{cases} \tag{15}$$

and substituting them into the relations

$$\begin{cases} Z_1 = \dfrac{1}{3}(Z^{(0)} + Z^{(+1)} + Z^{(-1)}) \\ Z_2 = \dfrac{1}{3}(Z^{(0)} + Z^{(+1)}\omega + Z^{(-1)}\omega^2) \\ Z_3 = \dfrac{1}{3}(Z^{(0)} + Z^{(+1)}\omega^2 + Z^{(-1)}\omega) \end{cases} \tag{16}$$

one can obtain the impedance matrix representing the Y junction

$$[Z] = \begin{pmatrix} Z_1 & Z_2 & Z_3 \\ Z_3 & Z_1 & Z_2 \\ Z_2 & Z_3 & Z_1 \end{pmatrix} \tag{17}$$

from which one can derive the input impedance normalized by the wave impedance Z_d of the coupled stripline

$$\bar{Z}_{in} = -1 - \frac{(Z_d + Z_1)^3 + Z_2^3 + Z_3^3 - 3(Z_d + Z_1)Z_2Z_3}{Z_d\{Z_2Z_3 - (Z_d + Z_1)^2\}}. \tag{18}$$

If the first circulation condition (10) is substituted into (18), it becomes

$$\bar{Z}_{in} = \frac{2}{1 - \dfrac{1}{\left\{\dfrac{\psi}{\pi}\dfrac{Z_e}{Z_d}\right\}^2 (h_0h_1 + h_1h_2 + h_2h_0)}}. \tag{19}$$

Moreover, if the second circulation condition (11) is satisfied, impedance matching is performed, and then $\bar{Z}_{in} = 1$.

As the two operations of the DCFO take place separately, each of them independently contributes to the input impedance at its circulation frequency. When the two circulation conditions are completely satisfied, the input impedance becomes equal to the wave impedance of the coupled stripline.

Now that the circulation adjustments are achieved, the last problem is to make the input impedance match the externally connected 50-Ω transmission line. It actually affects the overall circulator characteristics. It is, however, successfully performed using stripline tapers.

IV. The Experiments of DCFO

The DCFO has been demonstrated experimentally. The stripline Y-junction circulator used has almost the same geometry as that of a disk type, except that it is loaded with the ring ferrites. The ring ferrite is 20 mm in diameter, 2.5 mm thick with $r_1/r_2 = 0.45$. The ferrite material has a saturation magnetization of 950 G and a specific permittivity of 14.5. The junction coupling angle $2\psi = 0.8$ rad, and the thickness of the center conductor is 0.2 mm. The circulator is coupled to externally connected 50-Ω transmission lines through stripline tapers.

Fig. 9 shows examples of DCFO. In Fig. 9(a) are the circulator characteristics of the DCFO shown when the external magnetic field is changed sequentially. There are four cases shown with respect to different magnetic field intensities. The cases (1) and (2) show typically the double peaks of isolation though the insertion losses are not sufficiently low. In cases (3) and (4), a third peak appears additionally, and the insertion losses become lower over a broader frequency. Regarding this third peak, another higher mode is thought to be involved in the circulation. The figures of the externally applied magnetic field intensity H_{ex} (oersted) noted in Fig. 9 are obtained for the thickness

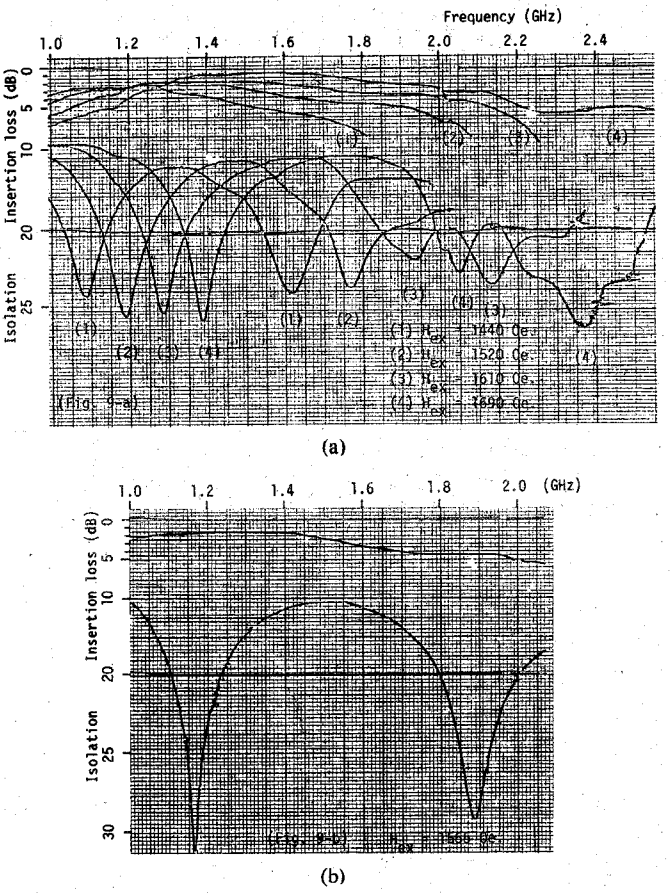

Fig. 9. Experimental examples of the DCFO. (a) The sequential performance of the DCFO when the external magnetic field H_{ex} (oersted) is changed. (b) The DCFO when the ring ferrite is surrounded with a dielectric of the specific permittivity $\varepsilon_d = 10$ and the width 10 mm.

0.2 mm of the center conductor, by exterpolation, from the measured data depending on the gap between the two ferrites. One can find that they are very strong in comparison with the figures of the external magnetic field in Fig. 2, which are measured directly between the magnet poles, free of ferrite.

In Fig. 9(b) is an example of the DCFO shown when the ferrite is surrounded with a dielectric material. From the experiments made on the circulator adjustments, we have found that it is effective to perform them by choosing the dielectric material surrounding the ferrite ring. If the dielectric constant of the material is changed, insertion loss and isolation characteristics are easily affected. It is also recognized that when the ratio r_1/r_2 is increased, the DCFO shifts to the higher frequency and less frequency difference is obtained. It agrees with the results that are observed with the resonance in the ring ferrite resonator.

V. Conclusion

The DCFO is demonstrated theoretically and experimentally. The explanation of the DCFO treated here is the simultaneous circulation of both mode 1 and mode 1A with the same direction of circulation. DCFO results when these two modes respectively satisfy their own second condition of perfect circulation. Several factors affecting the desired

circulator characteristics are the inner-to-outer radius ratio r_1/r_2, the saturation magnetization $4\pi M_s$, and the dielectric constant of the dielectric puck. Influences of these factors are not thoroughly discussed. It is, however, summarized that an increase of the ratio r_1/r_2 makes the frequency separation of DCFO small; less saturation magnetization causes the whole DCFO shift toward a high frequency as does a larger ratio of r_1/r_2.

The input impedance is the same as that of a SCFO. Therefore, it can be said that the design and operation of the DCFO circulator are given in almost the same manner with regard to the operation of mode 1, as is used for the disk-type circulator for SCFO use, because the operation of mode 1A is eventually determined.

According to these treatments, additionally, it is pointed out that higher order modes than mode 1A are possibly adjusted to be involved in circulation and a multiple circulation operation appears. Theoretical and experimental treatments of DCFO can be extended to the multiple circulation operation.

Now the author will try to speculate about the performance advantages possible with the DCFO approach compared to the conventional approach more commonly used, which is presented in [4] and [5]. As regards each SCFO among the DCFO, background physics and design principles for a SCFO circulator are rightly appreciated. They contain important ideas applicable to the DCFO performance. If some broad-banding networks are utilized [4], an overall DCFO performance will be improved. A broad-band performance produced in the process of circulation adjustments [5] can be practiced if the two curves of the second circulation condition nearly overlap over a broad frequency.

Apart from the discussions about such conventional approaches, the DCFO approach is expected to prepare the basis for theoretical and experimental treatments of various performances of DCFO. Among them, besides a normal performance of DCFO described in this paper, there is an inverse performance—diplexer operation—which involves both positive-sense and negative-sense modes. It contains an inverse circulation operation. The third is a broad-band performance. It appears when the bottom portion between the two peaks of isolation is elevated to the 20-dB level. The variety of these DCFO performances is promoted by adopting a multiple circulation operation.

Composites have not received much attention but the composites play essential roles in those various performances. Conductor, dielectric, and ferrite are constituents of composites (any conductor is not used in this paper). A combination of these constituents seems effective to make resonant modes in a composite change exquisitely and relevant circulation modes bring forth desirable effects, such as broad banding and impedance matching in addition to the aforementioned DCFO performances. A broad banding will be possible if one makes the two curves of the second circulation condition overlap over a much broader frequency. Impedance matching is important in circulator adjustments. To make the input impedance of the Y junction directly match the 50 Ω of the connected transmission lines is a short cut in the process of impedance matching.

Finally, one can say that these performances particularly depend on the permeability dispersion of ferrite, because a DCFO or a multiple circulation operation inherently involves many resonant modes and so many circulation modes ranging in the broad region of dispersion. Some of higher order circulation operations in the higher frequency are frequently observed to suffer from the ferromagnetic resonance absorption. To reduce absorption loss in the higher frequency, the use of low-loss ferrite and combination in composites must be considered.

Appendix
The EM Fields in the Dielectric–Ferrite Composite

Assume that the electric field intensity in the composite has only a z component and that the EM fields do not depend on the z coordinate. The specific permittivities of the dielectric puck and the ferrite ring are denoted by ε_1 and ε_2, respectively, and the specific gyrotropic permeability of the ferrite $[\mu]$, which is the tensor given by

$$[\mu] = \begin{pmatrix} \mu & -j\kappa & 0 \\ j\kappa & \mu & 0 \\ 0 & 0 & \mu_3 \end{pmatrix}. \tag{A1}$$

An effective specific permeability μ_e is given by

$$\mu_e = (\mu^2 - \kappa^2)/\mu \tag{A2}$$

and an intrinsic wave number k_2 in the ferrite by

$$k_2 = \omega\sqrt{\varepsilon_0\mu_0\varepsilon_2\mu_e} \tag{A3}$$

while in the dielectric puck by

$$k_1 = \omega\sqrt{\varepsilon_0\mu_0\varepsilon_1}. \tag{A4}$$

Of course, in the puck, the permeability has no gyrotropic factor.

With these definitions and assumptions, from Maxwell's equations in the cylindrical coordinates (r,θ,z), one can derive the electric fields in the dielectric puck

$$E_{z1} = \sum_{n=-\infty}^{\infty} a_n J_n(k_1 r) e^{-jn\theta} \tag{A5}$$

and in the ferrite ring

$$E_{z2} = \sum_{n=-\infty}^{\infty} b_n\{J_n(k_2 r) + c_n Y_n(k_2 r)\} e^{-jn\theta} \tag{A6}$$

where a_n, b_n, and c_n are coefficients. The radial and tangential components of the magnetic field intensity are related to E_z by, respectively,

$$H_r(r,\theta) = -j\left(\frac{1}{r}\frac{\partial E_z}{\partial \theta} + j\frac{\kappa}{\mu}\frac{\partial E_z}{\partial r}\right)/\omega\mu_0\mu_e \tag{A7}$$

$$H_\theta(r,\theta) = j\left(\frac{\partial E_z}{\partial r} - j\frac{\kappa}{\mu}\frac{1}{r}\frac{\partial E_z}{\partial \theta}\right)/\omega\mu_0\mu_e. \tag{A8}$$

While in the dielectric puck, those components of the magnetic field intensity are obtained by putting the second terms of (A7) and (A8) to zero and by taking $\mu_e = 1$.

The EM fields, both in the puck and in the ferrite ring, must satisfy the continuity condition with regard to tangential components of the EM fields at the boundary $r = r_1$, that is,

$$E_{z1} = E_{z2} \qquad H_{\theta 1} = H_{\theta 2}. \tag{A9}$$

Applying these continuity conditions at $r = r_1$, one can determine the coefficient c_n among (A5) and (A6). Now, one can rewrite the electric field solution in the ferrite ring as follows:

$$E_{z2} = \sum_{n=-\infty}^{\infty} b_n F_n e^{-jn\theta} \tag{A10}$$

$$F_n = J_n(x) + c_n Y_n(x) \tag{A11}$$

where

$$c_n = -\frac{J_n'(x_2) - J_n(x_2) I_n}{Y_n'(x_2) - Y_n(x_2) I_n} \qquad I_n = \frac{\eta_1}{\eta_2} \frac{J_n'(x_1)}{J_n(x_1)} + \frac{\kappa}{\mu} \frac{n}{x_2}$$

$$\frac{\eta_1}{\eta_2} = \frac{\sqrt{(\varepsilon_0 \varepsilon_1)/\mu_0}}{\sqrt{(\varepsilon_0 \varepsilon_2)/(\mu_0 \mu_2)}}$$

$$x = k_2 r$$

$$x_2 = k_2 r_1$$

$$x_1 = k_1 r_1. \tag{A12}$$

ACKNOWLEDGMENT

The author wishes to thank Z. Tanaka for his cooperation and S. Takata and K. Yokoyama of the TDK Electronics Company for their helpful discussions and support.

REFERENCES

[1] H. Bosma, "On the principle of stripline circulation," *Proc. IEE*, vol. 109, part B, suppl. 21, pp. 137–146, 1962.
[2] ——, "On stripline Y-circulation at UHF," *IEEE Trans. Microwave Theory Tech.*, vol. MTT-12, pp. 61–72, Jan. 1964.
[3] J. B. Davies and P. Cohen, "Theoretical design of symmetrical junction stripline circulator," *IEEE Trans. Microwave Theory Tech.*, vol. MTT-11, pp. 506–512, Nov. 1963.
[4] C. E. Fay and R. L. Comstock, "Operation of the ferrite junction circulator," *IEEE Trans. Microwave Theory Tech.*, vol. MTT-13, pp. 15–27, Jan. 1965.
[5] Y. S. Wu and F. J. Rosenbaum, "Wideband operation of microstrip circulators," *IEEE Trans. Microwave Theory Tech.*, vol. MTT-22, pp. 849–856, Oct. 1974.
[6] H. Bosma, "Junction circulators," in *Advances in Microwaves*, vol. 7, L. Young, Ed. New York: Academic, 1971.
[7] J. Brown and J. Clark, "A unique solid-state diplexer," *IRE Trans. Microwave Theory Tech.* (Corresp.), vol. MTT-10, p. 298, July 1962.
[8] L. v.d. Kint and E. Schanda, "Microwave quadruplexer," *IEEE Trans. Microwave Theory Tech.* (Corresp.), vol. MTT-11, pp. 90–92, Jan. 1963.
[9] T. Nagao, "Possibility of double circulation frequency operation of stripline Y-junction circulator," Proc. of *1975 IEEE-MTT-S International Microwave Symp.*, pp. 254–256, May 1975.
[10] D. Polder, "On the theory of ferromagnetic resonance," *Phil. Mag.*, vol. 40, pp. 99–115, Jan. 1949.
[11] K. Whiting, "Design data for UHF circulators," *IEEE Trans. Microwave Theory Tech.* (Corresp.), vol. MTT-15, pp. 195–198, Mar. 1968.
[12] J. K. Richardson, "An approximate formula for calculating Z_0 of a symmetric stripline," *IEEE Trans. Microwave Theory Tech.* (Corresp.), vol. MTT-15, pp. 130–131, Feb. 1967.